Article

Pyridine Ligand Rotation in Self-Assembled Trigonal Prisms. Evidence for Intracage Solvent Vapor Bubbles

Jaroslav Vacek, Douglas C. Caskey, Dominik Horinek, Richard K. Shoemaker, Peter J. Stang, and Josef Michl

J. Am. Chem. Soc., **2008**, 130 (24), 7629-7638 • DOI: 10.1021/ja801341m • Publication Date (Web): 21 May 2008

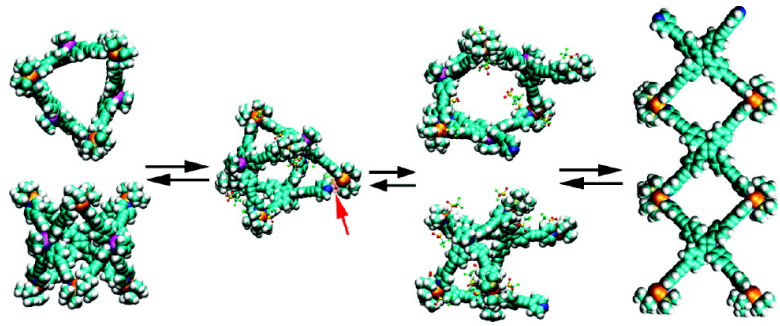

J|A|C|S
ARTICLES

Published on Web 05/21/2008

Pyridine Ligand Rotation in Self-Assembled Trigonal Prisms. Evidence for Intracage Solvent Vapor Bubbles

Jaroslav Vacek,*[,‡,§] Douglas C. Caskey,[‡] Dominik Horinek,[‡,||] Richard K. Shoemaker,[‡] Peter J. Stang,[†] and Josef Michl*[,‡,§]

Department of Chemistry, University of Utah, 315 South 1400 East, Room 2020, Salt Lake City, Utah 84112, Department of Chemistry and Biochemistry, University of Colorado, Boulder, Colorado 80309-0215, Institute of Organic Chemistry and Biochemistry, Academy of Sciences of the Czech Republic, 166 10 Prague 6, Czech Republic, and Department of Physics, Technische Universität München, 85748 Garching, Germany

Received November 29, 2007; E-mail: michl@eefus.colorado.edu; vacek@eefus.colorado.edu

Ⓦ **This paper contains enhanced objects available on the Internet at http://pubs.acs.org/jacs.**

Abstract: The rate of interconversion of the two inequivalent edges of the pyridine rings in the trigonal prism **3c**, self-assembled from 3 equiv of the star connector, tetrakis[4-(4-pyridylethynyl)phenyl]cyclobutadienecyclopentadienylcobalt, and 6 equiv of a platinum linker, *cis*-$(Me_3P)_2Pt^{2+}2TfO^-$, was determined by DNMR in nitromethane. It exhibits a highly unusual bilinear Eyring plot. In the low temperature regime, the activation enthalpy $\Delta H^{\ddagger}$ is ~12 kcal/mol and an activation entropy $\Delta S^{\ddagger}$ ranges from ~−15 to ~0 cal/mol·K as a function of the nature and concentration of the anions present. The reaction is attributed to hindered rotation of the pyridine rings about the Pt−N bond, facilitated by a tight pairing with a counterion. Above a counterion-dependent limiting temperature, $\Delta H^{\ddagger}$ and $\Delta S^{\ddagger}$ change abruptly to ~35 kcal/mol and ~60 cal/mol·K, respectively. The changes largely compensate, such that the reactions have comparable rates in the two regimes, both amenable to DNMR measurement, but their mechanisms clearly differ. Several kinetic models for the involvement of ion pairing equilibria fit the observed data nearly equally well, and they all contain a reaction step with high $\Delta H^{\ddagger}$ and $\Delta S^{\ddagger}$ values in the high-temperature regime. Its mechanism is proposed to involve a counterion-assisted reversible dissociation of one or two adjacent Pt−N bonds, followed by nearly free rotation of the terminal pyridine ring or rings and subsequent bond reclosure, which is similar to the last presumed step in the initial prism assembly. An interpretation of the very high $\Delta S^{\ddagger}$ value is suggested by molecular dynamics calculations: at equilibrium, there is a bubble of gaseous nitromethane solvent inside the prism, and it collapses when the prism opens as the transition state is reached. A simple calculation of the entropy of cavitation provides quantitative support for this tentative proposal. The presence of such voids might be generally important for the formation and properties of self-assembled cages.

Introduction

In the preceding companion paper[1] we described the self-assembly of the square connectors **1a**−**1d** and the linker **2** into the trigonal prisms **3a**−**3d** (Scheme 1). We provided a spectroscopic characterization of these molecular cages, discussed their chirality, and examined the rate of pyridine edge interchange in the prism faces by a combination of DNMR line shape fitting and 1-D EXCHSY NMR. The Eyring plots for the interchange in **3a**, **3b**, and **3d** yielded unexceptional activation parameters that fit expectations for a simple rotation of the pyridine rings about the Pt−N bond, except that the plot for **3d** contained a vague hint of nonlinearity. In contrast, the Eyring plot observed for **3c** was clearly bilinear and thus highly unusual. Activation parameters derived for **3c** in the low-temperature regime were comparable with those found for **3a**, **3b**, and **3d**. However, the $\Delta H^{\ddagger}$ and $\Delta S^{\ddagger}$ values derived for **3c** in the high-temperature region were exceptionally high, 35.1 ± 2.5 kcal/mol and 58.1 ± 8.1 cal/mol·K, respectively. The increase in $\Delta H^{\ddagger}$ relative to the low-temperature regime largely compensates the increase in $\Delta S^{\ddagger}$, such that the resulting rates in the low- and high-temperature regimes are not vastly different and both still fall into the limited range observable by DNMR.

The very rare bilinear nature of the Eyring plot hints at a change in the dominant mechanism in the pyridine edge exchange reaction in **3c** as a function of temperature, and it is possible that a similar phenomenon is responsible for the poor linearity of the Eyring plot for **3d**. We presently concentrate on **3c**, where the existence of two linear segments is unquestionable. If the low-temperature regime is characterized by the usual rotation of a pyridine moiety about the Pt−N bond, what is the mechanism that dominates in the high-temperature regime, and how can its high $\Delta H^{\ddagger}$ value, and, especially, its exceptionally high $\Delta S^{\ddagger}$ value, be accounted for?

[†] University of Utah.
[‡] University of Colorado.
[§] Academy of Sciences of the Czech Republic.
[||] Technische Universität München.

(1) Caskey, D. C.; Yamamoto, T.; Addicott, C.; Shoemaker, R. K.; Vacek, J.; Hawkridge, A. M.; Muddiman, D. C.; Kottas, G. S.; Michl, J.; Stang, P. J. *J. Am. Chem. Soc.* **2008**, *130*, 7620.

Scheme 1. Structures of Self-Assembled Trigonal Prisms[a]

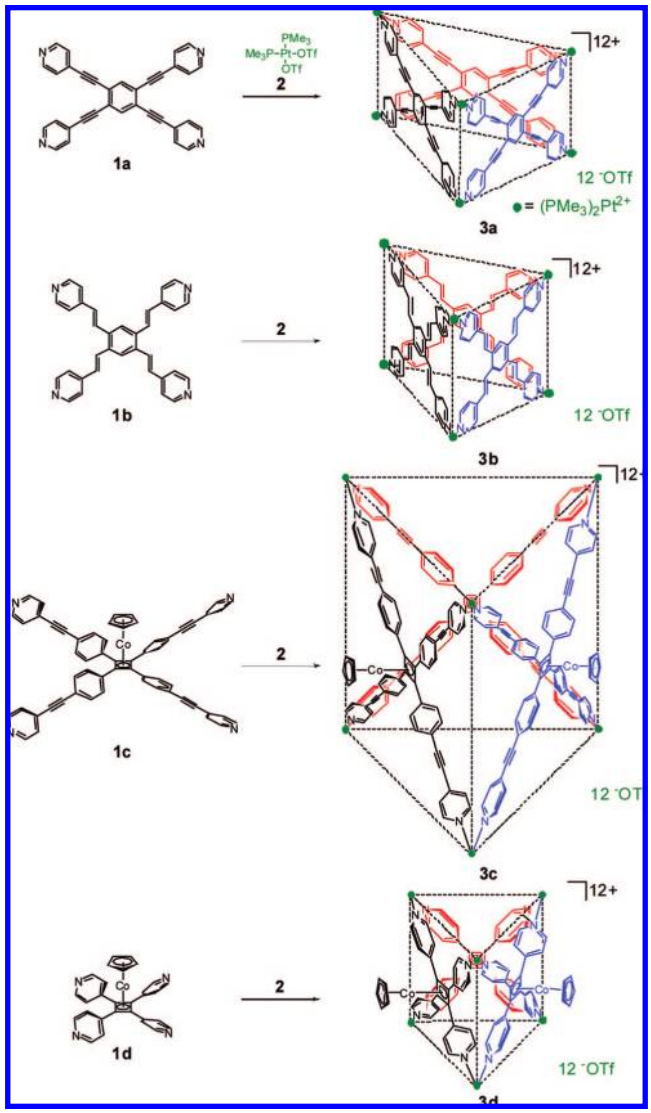

[a] Reproduced by permission from ref 1.

There are two simple ways in which a change in the mechanism could occur and various combinations of the two. (i) The "different path" limit. The same reactive species could have two parallel single-step reaction paths available to it, and their activation parameters $\Delta H^{\ddagger}$ and $\Delta S^{\ddagger}$ could be such that one of the paths would dominate at low and the other at high temperatures. (ii) The "different substrate" limit. There could be a rapid pre-equilibrium among more than one reactive species, all of whose NMR signals would be averaged to one set, and each of which would have only one single-step reaction path available to it. The $\Delta H°$ and $\Delta S°$ values that describe the equilibrium could be such that the reaction of one reactive species prevails at low temperatures and the reaction of another prevails at high temperatures. The most likely rapid pre-equilibrium that could affect the reactions of **3c** is ion pairing, and we have therefore examined the effects of the choice and concentration of counterions on the pyridine edge-exchange reaction. In the process, we made the intriguing discovery that even the standard pyridine ring rotation mechanism is subject to counterion effects and may not be as simple as it appears.

We have found that the Eyring plot remains bilinear under all conditions, and all detailed kinetic schemes we have been able to think of can be made to fit the observed rates only if they involve a step with a high $\Delta H^{\ddagger}$ and an exceptionally high $\Delta S^{\ddagger}$ value. It seems to us that the high $\Delta H^{\ddagger}$ value excludes mechanisms based on mere conformational changes and requires that a chemical bond be broken in the transition state. The weakest bonding in **3c** undoubtedly is the Pt−N coordination and the breaking of any one of these bonds would permit an essentially free rotation of the terminal pyridine ring. This sounds plausible, and Pt−N bond cleavage represents the reverse of the last anticipated step in prism self-assembly. However, why should the $\Delta S^{\ddagger}$ value be so extraordinarily high? We feel that only solvent involvement has a chance to account for it and look for inspiration in the results of molecular dynamics calculations. These produced a startling hint that we followed up to a point that allows us to make at least one tentative proposal that fits the unusual $\Delta S^{\ddagger}$ value. However, there may be other explanations that we have not thought of, and we recognize that much future testing will be required to find out if the interpretation we propose is indeed correct.

Results

Kinetics and Ion Pairing. Using the NMR techniques described earlier,[1] we expanded the collection of activation parameters available for the pyridine edge exchange reaction in the prism **3c** by (i) adding results for the pure undecamethylcarba-*closo*-dodecacarborate [1-H-$CB_{11}Me_{11}^{-}$] salt to those already available for the pure triflate salt and (ii) making measurements for solutions of **3c** salts to which various numbers of equivalents of Cs 1-H-$CB_{11}Me_{11}$ or Li triflate salt have been added (Table 1 and Figure 1). The highly methylated carborate anion was chosen for the lipophilic solubilizing properties of this class of anions[2] and for their tendency to adhere to metal cations,[3] in contrast to the triflate anion.

The observed rate constant of the carborate salt was unaffected by the addition of either excess cesium carborate or lithium triflate and the three bilinear Eyring plots coincide. The agreement of these three sets of independent measurements provides a measure of the reproducibility of the rate data. In contrast, the addition of excess lithium triflate to the triflate salt of **3c** changed all rate constants, while preserving the bilinear nature of all Eyring plots. Inspection of Figure 1 shows that the rate constants were increased in the low temperature regime and decreased in the high temperature regime. Remarkably, the two slopes in each Eyring plot for the triflates were hardly changed at all. The limited accuracy of the data does not allow definitive statements to be made about a possible absence of an often observed correlation between the $\Delta H^{\ddagger}$ and $\Delta S^{\ddagger}$ values.

Ion pairing of **3c** in nitromethane was investigated using diffusion-ordered (DOSY) NMR spectroscopy techniques described earlier,[1] and the results are summarized in Table 2.

Structural Calculations. Because of the size of the prism **3c** and the kinds of atoms contained in it, we have chosen molecular modeling based on the rather approximate UFF force field[4,5] implemented in the program TINK.[6] The structure of **3c** (Figure 2) was optimized with all CoCp moieties located outside the prism, an arrangement made highly probable by NMR evi-

(2) Valášek, M.; Pecka, J.; Jindřich, J.; Calleja, G.; Craig, P. R.; Michl, J. *J. Org. Chem.* **2005**, *70*, 405.
(3) Körbe, S.; Schreiber, P. J.; Michl, J. *Chem. Rev.* **2006**, *106*, 5208.
(4) Rappe, A. K.; Casewit, C. J.; Colwell, K. S.; Goddard, W. A., III; Skiff, W. M. *J. Am. Chem. Soc.* **1992**, *114*, 10024.
(5) Rappe, A. K.; Goddard, W. A., III. *J. Phys. Chem.* **1991**, *95*, 3358.
(6) Vacek, J.; Michl, J. *New J. Chem.* **1997**, *21*, 1259.

Table 1. Eyring Activation Parameters for Interconversion of Pyridine Edges in **3a**−**3d** in CD_3NO_2

		$\Delta H^{\ddagger}$, kcal/mol	$\Delta S^{\ddagger}$, cal/mol·K	R^2
3a 12 TfO^- [a]		12.4 (±2.1)	−16.1 (±5.5)	0.995
3b 12 TfO^- [a]		11.6 (±2.0)	−14.4 (±4.9)	0.994
3d 12 TfO^- [a]		13.2 (±2.2)	−13.2 (±4.5)	0.973
3c 12 TfO^- [a]	<∼318 K	11.1 (±1.9)	−17.5 (±6.0)	0.993
	>∼318 K	35.1 (±2.5)	58.1 (±8.1)	1.000
3c 30 TfO^-	<∼309 K	12.0 (±2.0)	−15.3 (±5.2)	0.997
	>∼309 K	32.2 (±2.1)	50.2 (±6.1)	1.000
3c 60 TfO^-	<∼303 K	13.8 (±2.3)	−9.8 (±3.3)	0.995
	>∼303 K	34.4 (±2.4)	58.1 (±8.1)	0.999
3c 12 $HCB_{11}Me_{11}^-$	<348 K	15.7 (±3.0)	−1.8 (±0.7)	1.000
	>348 K	37.7 (±2.6)	61.3 (±8.6)	1.000
3c 60 $HCB_{11}Me_{11}^-$	<348 K	15.6 (±3.0)	−2.2 (±0.8)	1.000
	>348 K	37.4 (±2.6)	60.5 (±8.5)	0.999
3c 12 $HCB_{11}Me_{11}^-$/12 TfO^-	<348 K	15.6 (±3.0)	−2.0 (±0.8)	0.999
	>348 K	38.6 (±2.7)	64.1 (±9.0)	0.998

[a] These results have been taken from ref 1.

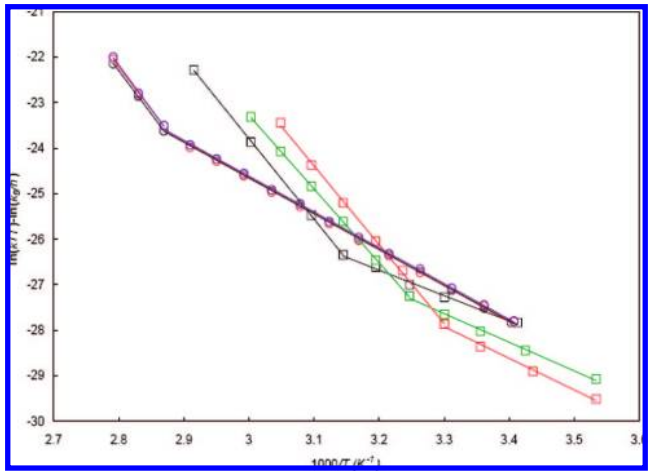

Figure 1. Eyring plots for pyridine edge interconversion rate constants in CD_3NO_2 for pure **3c**/12 TfO^- (empty black square), **3c**/12 $HCB_{11}Me_{11}^-$ (empty black circle), and for solutions of **3c** containing an added salt, with total anion concentrations 30 TfO^- (empty green square), 60 TfO^- (empty red square), 12 TfO^- + 12 $HCB_{11}Me_{11}^-$ (empty blue circle), and 60 $HCB_{11}Me_{11}^-$ (empty red circle). The three lines marked with empty circles coincide.

Table 2. Diffusion Coefficients for **3c**

cmpd	D^a
3c/12 OTf^-	1.9 ± 0.6
3c/12 $HCB_{11}Me_{11}^-$	1.6 ± 0.6, 4.9 ±0.6[b]
3c/12 $HCB_{11}Me_{11}^-$ + 12 OTf^-	1.6 ± 0.6, 5.0 ± 0.6[b]
Cs^+ $HCB_{11}Me_{11}^-$	7.6 ± 0.6[b]

[a] Diffusion coefficient in units of 10^{-10} m^2 s^{-1}, obtained from DOSY NMR measurements in CD_3NO_2 at 298 ± 0.25 K. The value of D observed for the pure solvent is 22.2 × 10^{-10} m^2 s^{-1} and the values observed for the solvent in the solutions of **3c** were in the range (16.0–19.5) × 10^{-10} m^2 s^{-1}. The effect of variation in viscosity can be at most equal to these differences, suggesting that a comparison of values in different rows of the table is dependable within an error of about ±13%. [b] Diffusion coefficient of $HCB_{11}Me_{11}^-$.

dence.[1] The rotational barrier around an intact Pt−N bond and the dissociation of a Pt−N bond of **3c** (Figure 2) were also examined. When the rotation of a pyridine ring relative to a platinum coordination plane was used to follow the reaction path in an isolated molecule, the barrier was found to be 21 kcal/mol. This value represents only an upper limit. Because of the approximate nature of the computational model and because the counterion (Table 1), and therefore also the solvent, most likely need to be included in the treatment of the rotation process, optimization of the geometry of the transition state was not considered worthwhile. This reaction deserves to be examined at a higher level of theory on a simpler model structure.

In an attempt to better distinguish whether one or two Pt−N bonds (on two adjacent Pt atoms) are likely to cleave, we also performed calculations in which 25 kcal/mol Morse bonds were used to describe two Pt−N bonds on adjacent vertices in the same square face, located in two different triangular faces. The choice of the Morse bond strength to use was not easy, since, to the best of our knowledge, the bond strength for a pyridine ligand on a platinum dication of the kind encountered in **3c** is not known. Extrapolation from values reported for Pt−N bonds in $Pt(I)(NH_3)$ complexes[7] and related complexes of other metals[8–10] suggested to us that a wide range from 15 to 35 kcal/mol is likely for pyridine in $Pt(II)L_2Py_2$, and the choice of 25 kcal/mol, although reasonable, is arbitrary.

We found that in an isolated molecule of **3c**, the breaking of the second Pt−N bond was facilitated by a release of ∼20 kcal/mol of strain energy introduced by the breaking of the first Pt−N bond. The structure with two broken bonds consists of three adjacent squares, i.e., an "unfolded prism" (Figure 2), and is extremely floppy.

Molecular Dynamics Calculations. In order to test the conjecture that the remarkable values of the activation entropy in Table 1 might be due to solvent effects, we also performed molecular dynamics calculations with explicit inclusion of solvent. A definitive molecular dynamics study of the solvation of the various forms of **3c** in nitromethane would require a careful optimization of the description of the pure solvent and of solvent–ion interactions, followed by a large number of trajectory calculations, perhaps involving constant temperature and pressure ensembles and Ewald summation of the electrostatic interactions. It would represent a whole separate project and lies outside the scope of the present paper. Currently, we are merely looking for qualitative guidance as to what the cause of the high $\Delta S^{\ddagger}$ value could be.

We performed ∼20 constant energy 500 ps molecular dynamics runs using the unadjusted universal force field (UFF) implemented in the program TINK[6] to describe the solvent and

(7) Liyanage, R.; Styles, M. L.; O'Hair, R. A. J.; Armentrout, P. B. *Int. J. Mass Spectrom.* **2003**, *227*, 47.
(8) Walter, D.; Armentrout, P. B. *J. Am. Chem. Soc.* **1998**, *120*, 3176.
(9) Rannulu, N. S.; Rodgers, M. T. *J. Phys. Chem. A* **2007**, *111*, 3465.
(10) Rodgers, M. T.; Stanley, J. R.; Amunugama, R. *J. Am. Chem. Soc.* **2000**, *122*, 10969.

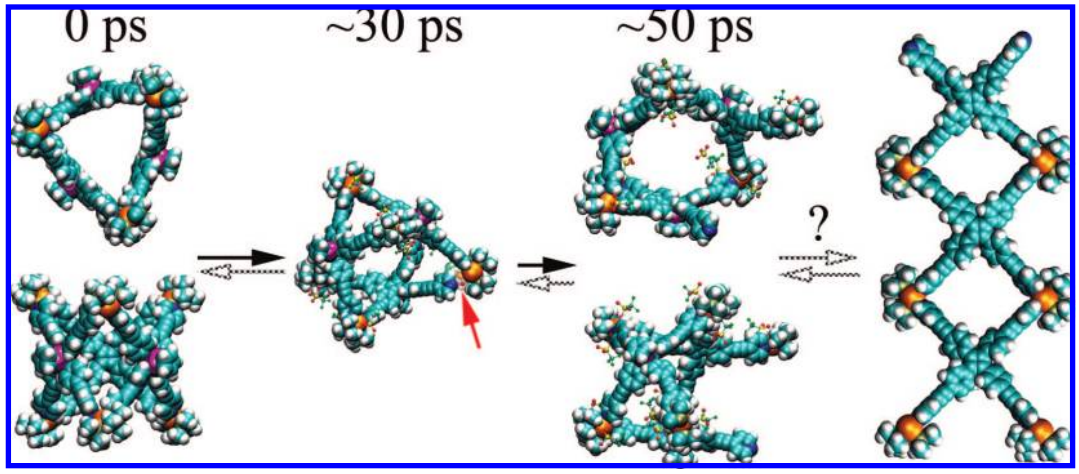

Figure 2. UFF optimized geometries of **3c** (see text). Color code: C, cyan; H, white; N, blue; Pt, orange; Co, purple; P, brown; O, red; S, yellow; F, green. Black horizontal arrows: transformations actually observed during a dynamics run in nitromethane solvent (not shown) at the times stated. White horizontal arrows: transformations anticipated. Red arrow: the breaking Pt−N bond.

the ions surrounding **3c**. Our objective was not so much to describe the course of the reaction in which the pyridine edges exchange but, rather, to obtain a qualitative picture of the typical solvation of **3c** at equilibrium and its solvation at a geometry with one broken Pt−N bond.

The equilibrium geometry was produced by starting with a system in which the solvent density was uniform inside and outside the prism and allowing it to relax. The broken bond geometry was arrived at by choosing two of the Pt−N bonds to be of the Morse type and 25 kcal/mol strong. The two bonds were formed by pyridine rings carried by the same square connector and were located at one of the three equivalent prism edges. The choice of bond strength has been rationalized above and makes the activation energy for a replacement of the Pt−N bond with a Pt−triflate bond small enough that this reaction actually took place within the duration of one of the runs. None of the runs reached a geometry with both Morse Pt−N bonds broken.

The prism **3c** was introduced at its separately optimized geometry and surrounded with 12 triflate anions located close to the six doubly positively charged platinum atoms with 48 to 1248 nitromethane solvent molecules located outside and inside the prism. Approximately 10−15 solvent molecules fit into the inner cavity. Figure 2 shows representative space-filling models of four different states of the prism. On the left is the optimized initial structure. The two central snapshots are taken during the one dynamics run in which a Pt−N bond broke, with solvent molecules deleted for clarity. The triflate counterions are shown in the "ball and stick fashion" for these two structures. The breaking of the Morse bond proceeded by coordination of one of the triflate counterions to a platinum atom accompanied by a stretching of the Pt−N distance. After some time, the Pt−N bond broke altogether and the Pt atom became square planar, with one pyridine and one triflate ligand. On the right of Figure 2 is the optimized structure of a solvent-free prism, two of whose adjacent Pt−N bonds have been broken. Such a fully opened prism is flat but extremely flexible.

The changes in solvation during the same dynamics run are shown in Figures 3–5. The three snapshots of **3c** were taken at the same instants as those of Figure 2, but now all the solvent molecules are shown. The structure is viewed once approximately parallel and once approximately perpendicular to the original 3-fold symmetry axis of the prism. In order to prevent the solvent molecules from completely obscuring the prism, only their bonds are shown ("wire model"). Those solvent molecules that are deemed to lie fully outside the internal prism cavity are shown in thin gray lines, the shade of gray becoming lighter as the molecule is located farther away from the viewer. Those that are deemed to lie at least partly inside the cavity are

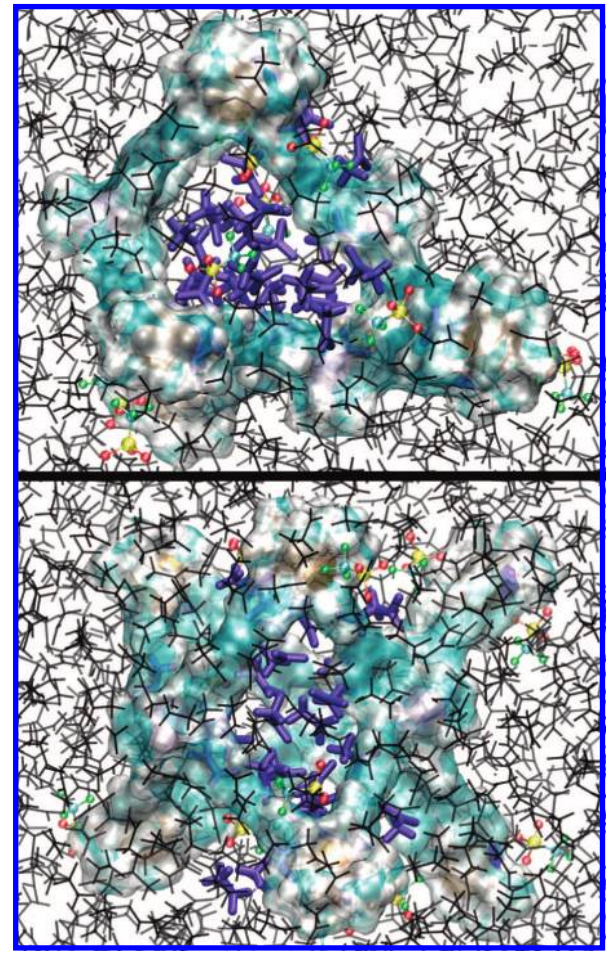

Figure 3. Representation of **3c** in nitromethane, with two Pt−N bonds of the Morse type (25 kcal/mol), after 3 ps of a dynamics run. Top, view roughly along the 3-fold axis. Bottom, view roughly perpendicular to the 3-fold axis (see text). For color code, see caption to Figure 2.

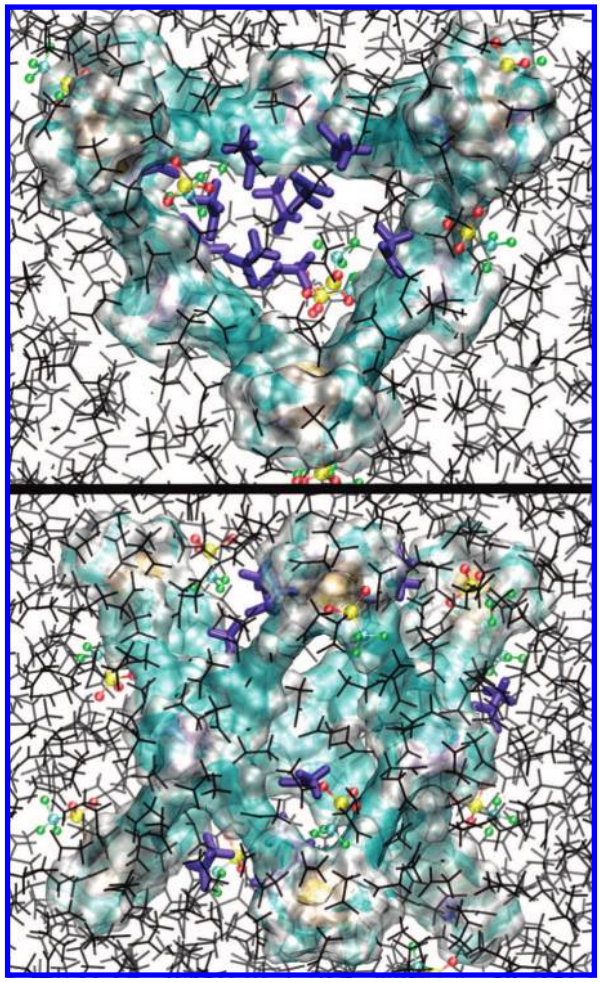

Figure 4. Representation of **3c** in nitromethane, with two Pt−N bonds of the Morse type (25 kcal/mol), after ~30 ps of a dynamics run. Top, view roughly along the 3-fold axis. Bottom, view roughly perpendicular to the 3-fold axis (see text). For color code, see caption to Figure 2.

Ⓦ A computer animation, available in the Web edition, displays the first ~30 s of the dynamics run, in which solvent molecules originally located inside the prism are shown in thick blue lines (for best viewing we recommend AppleQuicktime, www.apple.com/quicktime/).

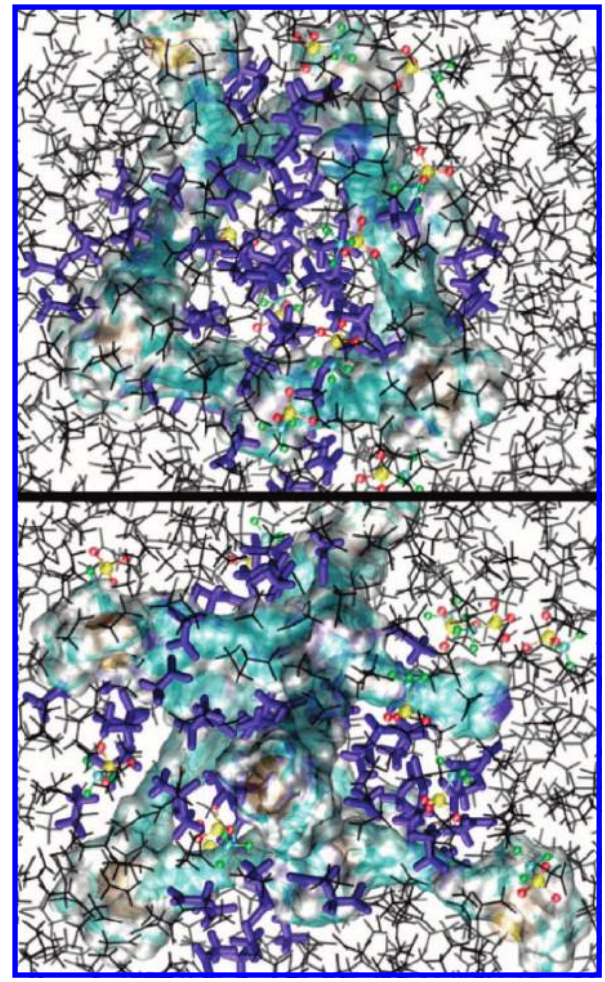

Figure 5. Representation of **3c** in nitromethane, with two Pt−N bonds of the Morse type (25 kcal/mol), after ~50 ps of a dynamics run. Top, view roughly along the 3-fold axis. Bottom, view roughly perpendicular to the 3-fold axis (see text). For color code, see caption to Figure 2.

Ⓦ A computer animation, available in the Web edition, displays a later phase of the dynamics run, after one of the edges broke (the opening is shown with a yellow circle) and solvent molecules enter the inside of the prism. Those solvent molecules that ultimately end up in the interior are shown in thick blue lines (for best viewing we recommend AppleQuicktime, www.apple.com/quicktime/).

shown in fat blue lines. The surface of the prism molecule **3c** itself is shown in a color-coded semitransparent representation. The triflate counterions are shown as color-coded ball-and-stick models.

In the first few picoseconds of each dynamics run (Figure 3), the solvent molecules reorient but remain packed inside the prism at approximately the same density as in the surrounding solvent (1.05–1.1 kg/L, obtained from the UFF simulation of pure nitromethane; the experimental density is 1.14,[11] and prior simulations gave values of 1.09[12] and 1.10[13] kg/L). However, after a few picoseconds the solvent molecules start to move out of the prism toward the charged vertices, while the triflate anions stay near their original positions close to the Pt ions. After a few dozen picoseconds the inside of the prism is essentially empty, with only a few molecules passing through occasionally (Figure 4), and the resulting vapor bubble has reached its maximum, after which it only fluctuates a little in time. At this point, the prism is extended to its maximum size. In the run represented, the prism subsequently opened at one of the vertices, with a triflate anion replacing the pyridine ligand at the platinum atom. At the same time, the solvent refilled the void and the vapor bubble disappeared (Figure 5). By clicking in Figure 4 in the Web edition, the reader can activate a computer animation that displays the result of one of the molecular dynamics runs for the initial formation of the vapor bubble upon equilibration. Clicking in Figure 5 activates a computer animation that shows the subsequent collapse of the bubble caused by Pt−N bond breaking as the same molecular dynamics run is continued.

Entropy of Cavitation in Nitromethane. To follow up on the hint provided by the results of molecular dynamics calculations and test the possibility that the highly unusual observed value of $\Delta S^{\ddagger}$ is due to the collapse at the transition state of a bubble of gaseous solvent that is present inside the prism **3c** at equilibrium, we needed a semiquantitative estimate of the gain

(11) Lide, D. R. *Handbook of Chemistry and Physics*, 78th ed.; CRC Press: New York, 1997.
(12) Sorescu, D. C.; Rice, B. M.; Thompson, D. L. *J. Phys. Chem. A* **2001**, *105*, 9336.
(13) Liu, H.; Zhao, J.; Ji, G.; Gong, Z.; Wei, D. *Physica B* **2006**, *382*, 334.

in entropy associated with the formation of such a bubble in the nitromethane solvent.

The solvation thermodynamics of hydrophobic cavities has not been studied in nitromethane to our knowledge but has been extensively studied in water.[14–16] In water, different explanations for the hydrophobic effect have been envisioned. The classic iceberg model[17] relates the loss of entropy to the formation of a cage-like first solvation shell of a cavity. While there is still some debate on the nature of the entropy loss, a common view is that it is related to the difficulty of accommodating a cavity in liquid water without disrupting the hydrogen bonding network present.[18] This effect dominates the free energy of solvation for cavities with radii below 1 nm.[14] We do not know if nitromethane behaves similarly.

Nevertheless, an evaluation of the excluded volume entropy yields a simple estimate of the solvent contribution to the $\Delta S^{\ddagger}$ of our reaction. The free energy change that occurs when a cavity of volume V is established in a liquid is related to the probability of finding such a cavity in the solvent as a result of density fluctuations. In analogy to the theory of hydrophobic solvation,[19] we obtain the free energy from the expression

$$G = kT\rho^2 V^2/2\alpha + kT(\ln 2\pi\alpha)/2 \qquad (1)$$

Here, ρ is the density of the solvent and α is the mean fluctuation of solvent molecules in a volume V. The nitromethane molecules were approximated as spheres centered at their nitrogen atoms. Using this assumption, α is given as[14]

$$\alpha = \rho V + \rho^2 \int_V d\boldsymbol{r} \int_V d\boldsymbol{r}'[g_{NN}(|\boldsymbol{r} - \boldsymbol{r}'|) - 1] \qquad (2)$$

where $g_{NN}(r)$ is the radial distribution function of the nitrogen atoms. This function was calculated from the molecular dynamics run for the pure bulk liquid in a spherical volume of ~7 nm^3 at a density of 1.05 kg/L using standard procedures,[20] and the result is shown in Figure 6. The usual behavior of a liquid is observed, with a well-defined peak at $r = 5$ Å and decaying oscillations for larger r. Less well converged but similar radial distribution functions were published in 2007 using the CHARMM force field and an NPT statistical ensemble.[13]

For an accurate calculation of α, the exact shape of the cavity would be required. For our purposes, we assumed the cavity to be spherical, in which case the integration required for the calculation of α becomes one-dimensional.[21] The bubble cavitation entropy $\Delta S = -\Delta G/T$ was calculated as a function of the bubble radius R and is shown in Figure 6.

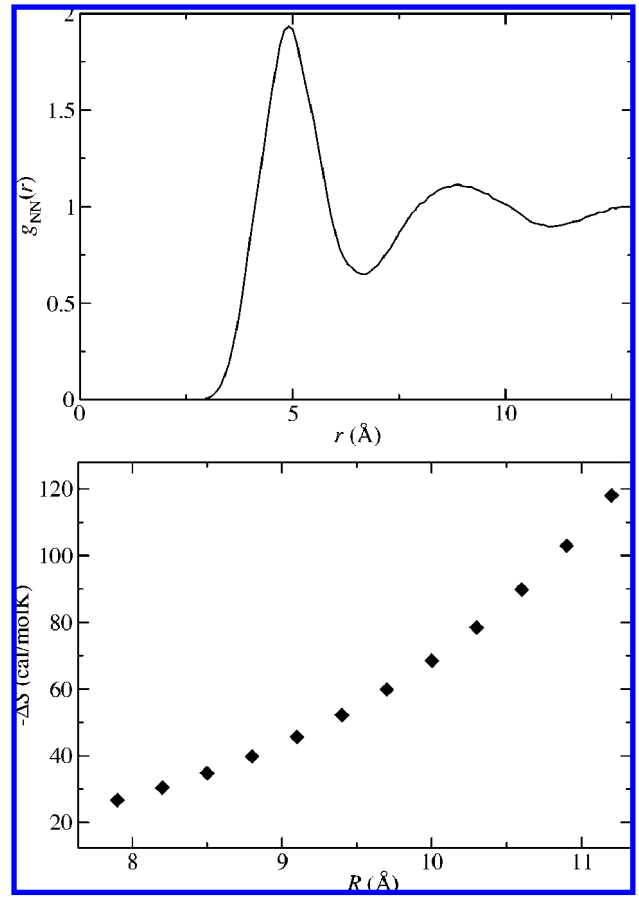

Figure 6. Top: Radial distribution function $g_{NN}(r)$ of the nitrogen atoms in liquid nitromethane from molecular dynamics simulations. Bottom: entropy of bubble formation as a function of its radius estimated from $g_{NN}(r)$ using eq 1.

Discussion

Pyridine Ligand Edge Exchange Kinetics (Table 1, Figure 1). Because each prism contains 12 pyridine rings whose rotations need not be independent, a full kinetic analysis would require far more experimental information than is readily accessible. We shall assume that in **3c** each pyridine rotates independently of the others and shall address two issues.

First, we deal with the "ordinary" pyridine rotation mechanism believed to dominate in the low-temperature regime. Clearly, it is not as simple as generally assumed, since its rate is quite sensitive to the nature of the counterion. We found considerable sensitivity to the counterion concentration in the case of triflate and none in the case of the 1-H-$CB_{11}Me_{11}^-$ anion. We have not examined the prisms **3a**, **3b**, and **3d** in this regard, but it is likely that the state of ion pairing has an effect on the ease of pyridine ligand rotation in general and will need to be carefully controlled in future studies of such rotation.

Second, we deal with the "extraordinary" pyridine rotation mechanism that prevails in **3c** at higher temperatures. Since the 1-H-$CB_{11}Me_{11}^-$ salt of **3c**, which shows no indication of counterion effects and is therefore presumably always present in the same state of ion pairing, still displays a bilinear Eyring plot similar to the others, it appears that the pyridine edge exchange reaction can occur by two different mechanisms that differ in a more profound way than just by the state of ion pairing ("different path" limit in the sense described in the Introduction).

Low-Temperature Regime. We have already noted[1] that the enthalpies ($\Delta H^{\ddagger}$) and entropies ($\Delta S^{\ddagger}$) of activation for the pyridine edge exchange reaction in the triflate salts of **3a**, **3b**, and **3d**, whose Eyring plots can be fitted with a single straight line, are all identical within our experimental accuracy (Table 1), are similar to prior literature data,[22] and lie within the error bar of those found for the low temperature process in the triflate of **3c**. They all fit expectations for the normally assumed

(14) Chandler, D. *Nature* **2005**, *437*, 640.
(15) Ben-Amotz, D. *J. Chem. Phys.* **2005**, *123*, 184504.
(16) Choudhury, N.; Pettitt, B. M. *J. Am. Chem. Soc.* **2007**, *129*, 4847.
(17) Frank, H. S.; Evans, M. W. *J. Chem. Phys.* **1945**, *13*, 507.
(18) Ball, P. *Chem. Rev.* **2008**, *108*, 74.
(19) Hummer, G.; Garde, S.; Garcia, A. E.; Pohorille, A.; Pratt, L. R. *Proc. Natl. Acad. Sci. U.S.A.* **1996**, *93*, 8951.
(20) Allen, M. P.; Tildesley, D. J. *Computer Simulations of Liquids*; Clarendon Press: Oxford, 1987.
(21) Hill, T. L. *J. Phys. Chem.* **1958**, *28*, 1179.

mechanism of pyridine edge exchange by rotation around an intact Pt−N bond.

However, the presently observed counterion dependence and common ion effects observed with **3c** suggest that the reaction involves more than a simple rotation (Table 1 and Figure 1). The results show that the nature and the concentration of counterions in the solution have a limited effect on the slope of the linear plot, which is only a little higher for the carborate than for the triflate salt. However, they affect the rate at any one temperature considerably. The determination of the $\Delta H^{\ddagger}$ and $\Delta S^{\ddagger}$ values requires a long extrapolation and results in large error margins, making general statements difficult. These values appear to be mutually correlated in a way that results in a compensation of their effect on the reaction rate. However, the accuracy of the data, limited by the accessible range of temperatures, is insufficient for a detailed analysis of the origin of the apparent correlation, which could be meaningful or simply arise from the statistical nature of linear least-squares regression.[23,24]

The interpretation that we find most plausible is to postulate that the pyridine edge exchange reaction occurs only upon tight ion pairing by the platinum cation whose ligand undergoes rotation. If a particular combination of ion pair stoichiometry and structure dominates in the solution equilibrium, it will dictate the activation parameters. Even if several ion pair combinations of stoichiometry and structure coexist, as long as ion pair equilibria are established much faster than the pyridine rings rotate, the NMR spectra of all species related by ion pairing will be averaged and the observed reaction rate will be the weighted average over all reacting types of ion pair species present. If the reactions involve ion pairing pre-equilibria and are not single-step processes, the $\Delta H^{\ddagger}$ and $\Delta S^{\ddagger}$ values deduced from data shown in Figure 1 are only apparent and reflect the temperature dependence of all pre-equilibria in addition to that of the actual rotation step.

Why should pyridine rings carried by a free vertex of type $[L_2L'_2Pt^{2+}]$ exhibit different rates for edge exchange by rotation around the Pt−N bond than those attached to a singly $[L_2L_2' Pt^{2+} X^-]$ or doubly $[L_2L_2' Pt^{2+} 2X^-]$ tightly ion paired vertex, where X^- is the counterion, yet show similar Eyring plot slopes? Considerable additional experimentation and/or computation will be needed before a definitive answer can be found, but a first qualitative rationalization that comes to mind is that the preference of the Pt atom for a perpendicular alignment of its pyridine ligands is diminished in the presence of a tightly attached counterion, which acts as a weakly coordinated fifth ligand. If the rotation only takes place rapidly when such a fifth ligand is present but it does not matter much what the ligand is, $\Delta H^{\ddagger}$ will remain more or less the same in all cases. If nearly all of the vertex cations exist as a tight ion pair with the anion X^-, such as $[L_2L_2' Pt^{2+} X^-]$, the fifth ligand is always present. The reaction is then monomolecular, and $\Delta S^{\ddagger}$ has a corresponding value, which should be close to zero. However, if X^- needs to be brought from solution first, a bimolecular step is involved, and $\Delta S^{\ddagger}$ should be more negative. This would clearly be the case if the cation is in the form $[L_2L'_2Pt^{2+}]$. However, this line of qualitative argument does not make it obvious whether the doubly ion paired form $[L_2L_2' Pt^{2+} 2X^-]$ would be even more favorable for the reaction than the singly paired form $[L_2L_2' Pt^{2+} X^-]$.

Since the reaction rate of the 1-H-$CB_{11}Me_{11}^-$ salt is unaffected by the presence of additional 1-H-$CB_{11}Me_{11}^-$, there is no reason to postulate that it is present in more than one ion paired form. Some statements about ion pairing can be made based on the measured diffusion coefficients.[25] The 1-H-$CB_{11}Me_{11}^-$ anion is surely paired with **3c** to some degree, since the measured diffusion constant of its salt with **3c** is only 4.9×10^{-10} m^2 s^{-1}, while that of its cesium salt is 7.6×10^{-10} m^2 s^{-1} (Table 2). However, it is also clear that some of the carborate anion remains unpaired and free to move independently of the **3c** cations, since its diffusion coefficient is much higher than that of **3c** (1.6×10^{-10} m^2 s^{-1}). Thus, it appears that this carborate salt is present essentially only in the form $[L_2L_2' Pt^{2+} X^-]$ on each vertex and that its activation parameters have a simple significance. If the above proposal is correct, a $\Delta S^{\ddagger}$ value near zero appears perfectly reasonable for a simple rotation around the Pt−N bond.

The case of the triflate salt of **3c** is more complicated because Figure 1 suggests that ion pairing equilibria definitely need to be invoked. The kinetic scheme need not be simple, but the results (Table 1) fit the above proposal qualitatively. The apparent $\Delta S^{\ddagger}$ value for the pyridine edge exchange process is now much more negative. Although the effect of the addition of excess triflate is small relative to the error bars, it appears to increase $\Delta S^{\ddagger}$, bringing it closer to the carborate value. At the same time, the $\Delta H^{\ddagger}$ value also stays constant within error bars but appears to increase sufficiently for the reaction rate constant to be unmistakably reduced (Figure 1). If the above proposal for the interpretation of the effect of ion pairing on the $\Delta S^{\ddagger}$ value is correct, **3c** triflate has a more negative value because it is largely present in a dissociated form, presumably $[L_2L_2' Pt^{2+}]$. In order to react, $[L_2L_2' Pt^{2+}]$ requires a bimolecular approach of a triflate anion to form a pentacoordinate reactive species $[L_2L_2' Pt^{2+} X^-]$. A more quantitative analysis requires a separation of the temperature dependence of the triflate ion pairing equilibrium from the temperature dependence of the reaction rate proper, and we shall return to it briefly below for both temperature regimes simultaneously.

The experimental information available does not allow us to claim with certainty that **3c** triflate is indeed present as a mixture of the $[L_2L_2' Pt^{2+}]$ and $[L_2L_2' Pt^{2+} X^-]$ forms, but it appears plausible. Since neither the reaction rate of the 1-H-$CB_{11}Me_{11}^-$ salt (Table 5) nor the diffusion coefficient of its cation and anion (Table 2) is affected by the addition of lithium triflate, we conclude that triflate does not displace the carborane anion from the platinum cation, in keeping with the considerable affinity of methylated carborate anions for metal cations[3] and with the expected poorer solvation of these highly lipophilic anions in the polar nitromethane solvent, relative to triflate. Since we believe that the carborate salt is present as singly ion paired species $[L_2L_2'Pt^{2+} X^-]$, it would appear likely although not proven that the less firmly bound triflate is present as a mixture of $[L_2L_2'Pt^{2+}]$ and $[L_2L_2'Pt^{2+} X^-]$.

Finally, we note that the addition of a fifth ligand to the platinum atom is well known as the beginning of ligand

(22) Tárkányi, G.; Jude, H.; Pálinkás, G.; Stang, P. J. *Org. Lett.* **2005**, *7*, 4971.

(23) Krug, R. R.; Hunter, W. G.; Grieger, R. A. *J. Phys. Chem.* **1976**, *80*, 2335.

(24) For a very relevant example of such an analysis for reaction enthalpies $\Delta H°$ and entropies $\Delta S°$, see: Leung, D. H.; Bergman, R. G.; Raymond, K. N. *J. Am. Chem. Soc.* **2008**, *130*, 2798.

(25) For a recent example of such analysis and additional references, see: Pluth, M. D.; Tiedemann, B. E. F.; van Halbeek, H.; Nunlist, R.; Raymond, K. N. *Inorg. Chem.* **2008**, *47*, 1411.

substitution by the associative mechanism[26,27] and recognized as weakening the bonds initially present. It is therefore plausible that it should reduce the preference of a ligand such as pyridine for a particular orientation relative to the NPtN plane. One could imagine that the effect of the fifth ligand goes farther and that it may actually induce ligand substitution. This is the subject we take up next.

High-Temperature Regime. So far, we have considered the low-temperature limiting behavior in the pyridine rotation in **3c**, which does not appear to differ significantly from that in the other prisms **3**. Next, we need to consider the high-temperature regime in the unusual bilinear Eyring plot for **3c** and its very strange values of the activation parameters.

We recall that the carborate salt of **3c** shows no counterion effects on either straight line segment in the Eyring plot, such that it does not appear justified to invoke ion pair equilibria to explain its bilinear nature. We therefore assume that its activation parameters are those for a kinetically one-step reaction of a single species. The simplest assumption is to propose that in the low- and the high-temperature limits, this species interchanges its pyridine edges by two different parallel mechanisms, characterized by two different sets of $\Delta H^{\ddagger}$ and $\Delta S^{\ddagger}$ values. As we have just discussed, ordinary rotation around the Pt−N bond is believed to dominate in the low-temperature limit for which these values are unexceptional. Based on the arguments given, the reacting species appears to be the singly paired ion $[L_2L_2'Pt^{2+}\ X^-]$, where $X^- = 1\text{-H-}CB_{11}Me_{11}^-$.

The dominant mechanism used by this species at high temperatures has a much higher $\Delta H^{\ddagger}$ of ~38 kcal/mol and also an incredibly high $\Delta S^{\ddagger}$ of ~62 cal/mol·K. The $\Delta H^{\ddagger}$ value does not fit a mere conformational change and demands that a real chemical bond, or perhaps even two, be broken in the transition state. A likely candidate is a reversible cleavage of one Pt−N bond or possibly two adjacent Pt−N bonds to form a partially or fully open prism, which would allow a nearly free pyridyl rotation at the end of a free arm or arms in the transition state. The liberated site on the platinum cation would presumably be simultaneously occupied by another ligand, perhaps a molecule of the solvent, but, more likely, a counterion already present in a tight ion pair or brought up from solution. Such a coordination bond breaking process is plausible in principle, since it is the reverse of the presumed last step in the original self-assembly of the prism, performed under reversible conditions.

Within the very poor state of existing knowledge of the bond strengths for the pyridine ligand on platinum dication discussed above, the observed $\Delta H^{\ddagger}$ values (Table 1) appear to be of the right order of magnitude for breaking not only one but probably two Pt−N bonds, assuming that the coordination energy of one of the methyl groups of the carborate anion to the Pt cation that replaces the pyridine in the transition state is on the order of 10−15 kcal/mol. Such a value can be very roughly guessed by analogy to the results calculated[28] for the interaction of the $CB_{11}Me_{12}^-$ anion with the Me_3Sn^+ and Me_3Ge^+ cations.

The huge positive values of $\Delta S^{\ddagger}$ (Table 1) are totally out of line with those normally observed for the simple bond cleavage dissociation of ion−ligand complexes, which are also positive, but six times smaller.[29] Even if two bonds are breaking in our postulated transition state, and even after we take into account the floppiness of the opened prism, the observed values appear entirely unreasonable without attributing an essential role to the solvent. Very large positive values of $\Delta S^{\ddagger}$ are nearly but not totally without precedent, as they have been found for protein folding and unfolding processes. The unfolding of elongation factor 2 (EF2) proteins from psychrotolerant and thermophilic Archaea proceeds with $\Delta S^{\ddagger}$ values ranging from 142 to 414 cal/mol·K,[30] which dwarf the one observed here. The unfolding of the extracellular serine protease, α-lytic protease (αLP) has been characterized by a $\Delta S^{\ddagger}$ of 79 cal/mol·K.[31] In these processes, the solvent surely plays an essential role, and they are not simple one-step events.

Next, we consider the results for the triflate salt of **3c**. In the high temperature regime, both $\Delta H^{\ddagger}$ and $\Delta S^{\ddagger}$ are somewhat affected by the addition of triflate ions, but their values are within the uncertainty of those for the carborate salt. However, in the observed range of temperatures, the rate constants clearly increase as triflate concentration increases, and this is the opposite of what is observed in the low-temperature regime. As in the low-temperature regime, more than one species appears to be involved, presumably pyridines attached to differently ion paired Pt atoms, and we are again led to the tentative conclusion that these are $[L_2L_2'Pt^{2+}]$ and $[L_2L_2'\ Pt^{2+}\ X^-]$.

A detailed interpretation of the data for triflates therefore calls for a fitting to a kinetic scheme, and the two temperature regimes should be fitted simultaneously. At a minimum, we need to include a temperature dependent ion pairing equilibrium between $[L_2L_2'\ Pt^{2+}]$ and $[L_2L_2'\ Pt^{2+}\ X^-]$ and two distinct pyridine edge exchange mechanisms in the latter, with different activation parameters. However, there are many possible schemes, because in principle $[L_2L_2'\ Pt^{2+}]$, $[L_2L_2'\ Pt^{2+}\ X^-]$, and $[L_2L_2'\ Pt^{2+}\ 2X^-]$ could all be reactive; each could react by one of two mechanisms, and each reaction could require an additional triflate anion, or even two anions on two adjacent vertices. Nonlinear least-squares fitting to all rates observed for triflate salts simultaneously was performed for several such schemes. Unfortunately, the quality and quantity of our kinetic data are such that a reasonably satisfactory agreement was obtained for almost any such scheme, and we cannot reliably differentiate between them. The only conclusion we have been able to reach from this exercise is that, for the triflate salt, as for the carborate salt, in any of the schemes the high-temperature limit involves a reaction step with a high value of $\Delta H^{\ddagger}$ and a quite extraordinarily high value of $\Delta S^{\ddagger}$.

High $\Delta S^{\ddagger}$ Value in the High-Temperature Regime. A rational explanation of the high $\Delta H^{\ddagger}$ value is that two adjacent Pt−N bonds, or perhaps one such bond, are broken in the transition state and replaced by much weaker interactions of the Pt cation with its counterion in one of the four square planar coordination sites, as suggested by the molecular dynamics simulation. We do not have a similarly ordinary rationalization of the high $\Delta S^{\ddagger}$ value, which makes the reaction observable at the moderate temperatures used, in spite of its very high activation enthalpy. Although a partially or fully open prism is very floppy, this in

(26) Basolo, F.; Pearson, R. G. *Mechanisms of Inorganic Reactions: A Study of Metal Complexes in Solution*, 2nd ed.; Wiley: New York, 1967; Chapter 5, pp 351–453.
(27) Sykes, A. G. *Kinetics of Inorganic Reactions*; Pergamon Press: Oxford, 1966; Chapter 13, pp 250–261.
(28) Zharov, I.; Weng, T.; Orendt, A. M.; Barich, D. H.; Penner-Hahn, J.; Grant, D. M.; Havlas, Z.; Michl, J. *J. Am. Chem. Soc.* **2004**, *126*, 12033.
(29) Lifshitz, C. *Adv. Mass Spectrom.* **1989**, *11*, 113.
(30) Siddiqui, K. S.; Cavicchioli, R.; Thomas, T. *Extremophiles* **2002**, *6*, 143.
(31) Jaswal, S. S.; Truhlar, S. M. E.; Dill, K. A.; Agard, D. A. *J. Mol. Biol.* **2005**, *347*, 355.

itself can hardly account for a value that would normally be expected only if the prism disintegrated into several freely floating fragments. We also find it difficult to understand how changes in ion pairing upon reaching the transition state could account for the observed value. Invoking cooperativity effects that would invalidate our assumption of independent rotation of the pyridine rings present does not seem to help either, since they would normally make $\Delta S^{\ddagger}$ more negative, not more positive.

If the hint provided by the molecular dynamics calculations is correct, at equilibrium a bubble of solvent vapor is present inside the prism **3c** (Figure 4), and the prism is stretched to its maximum size by the mutual repulsion of the six positively charged vertices through an environment whose dielectric constant is nearly exactly unity. The cleavage of one or two Pt−N bonds on the way to the transition state with a freely rotating pyridine ring or rings is accompanied with an expansion of the solvent into the bubble (Figure 5), which should indeed contribute a large amount of positive entropy. The observed $\Delta S^{\ddagger}$ of ∼60 cal/mol·K, combined with the approximate evaluation of the excluded-volume entropy as a function of bubble size (Figure 6), corresponds to a bubble radius close to 1 nm and a volume of 3.9 nm^3. This result can be compared with the 3.6 ± 0.5 nm^3 internal volume of **3c** estimated from the molecular dynamics simulations and makes us propose that this is indeed the most plausible interpretation of the data. The perfect coincidence of the volumes deduced from $\Delta S^{\ddagger}$ and from the size of the caged bubble is undoubtedly accidental. A proper quantitative analysis of the thermodynamics of bubble formation and destruction would require an improvement of the simulation method, an accurate description of the shape of the bubble, and an evaluation of entropy contributions from solvent orientation. It would also need to explicitly recognize that three of the five walls of the bubble are formed not by the solvent, but by the tetragonal connectors that form the prism.

Even though NMR evidence argues against it, we cannot exclude the possibility that in the real structure of **3c** the cyclopentadienyl residues are turned toward the inside of the prism, instead of the outside. The bubble would then be partly filled by the cyclopentadienyl rings, but the inside of the prism would remain nonpolar. We believe that although this would reduce the volume available inside the prism and remove the quantitative agreement noted above, it would still not change the situation in a fundamental way.

The dewetting of the inside of the prism at equilibrium presumably results from a combination of the nonpolar structure of its walls and the highly polar doubly charged vertices, which makes **3c** amphiphilic and apparently makes it impossible for the highly polar solvent to assume a favorable arrangement inside. A comparison can be made with hydrophobic effects and cavitation in water, where such phenomena are much more common and about which much more is known.[14–16] The presently proposed bubble in the highly polar nitromethane could then be said to originate in an analogous solvophobic effect. In water, small hydrophobic solutes are wet, with the solvent packed close to their surface, but large ones are dewetted, with water staying up to 4 Å away from their surfaces. At room temperature, the entropy of formation of cavities in water is negative for diameters up to about 1 nm and positive for larger cavities. For diameters close to 6 Å, it is ∼ −35 cal/mol·K. At lower temperatures it can be as much as −60 cal/mol·K.[15]

Caged Vapor Bubbles? It is natural to ask how general the appearance of voids inside various molecular cages in various solvents might be. Of course, there are empty cavities inside molecules such as the fullerenes. However, the walls of such cages are quite hard to penetrate, and the solvent molecules cannot travel between the voids and the solvent. There also is quite convincing evidence that an otherwise accessible void in a molecular cage can develop when the solvent molecules become too large to fit inside.[32] However, in the situation encountered with **3c** in nitromethane the solvent molecules are free to enter and exit the cage without significant steric hindrance, and ample space is available to them inside. Thus, the drying of the cage more closely resembles the formation of a nanobubble in a solid-state nanopore[33] or the dewetting transition during protein folding.[34] Perhaps the similarity between the high $\Delta S^{\ddagger}$ for protein unfolding[30,31] and the high $\Delta S^{\ddagger}$ observed for the opening of **3c** is not accidental, and the reversible self-assembly of **3c** in nitromethane represents a simple analogue to the folding of proteins in water.

It is conceivable that vapor bubbles occur in many of the self-assembled cages that have been studied over the years and simply have escaped detection, but it is also possible that the conditions for their existence are met only rarely and that **3c** in nitromethane is exceptional. The ease of template-free assembly of the cages **3** in nitromethane, but less readily in chloroform and methylene chloride, may be related to solvophobic aggregation. A closer examination of **3c** and other cages by a series of computational and experimental tests is easily envisaged but lies beyond the scope of this paper.

Conclusions

Counterion effects and the bilinear Eyring plot exhibited by the pyridine edge interchange reaction in **3c** have been examined. The results suggest that the ordinary reaction mechanism, rotation around the Pt−N bond, proceeds after association of the counterion with the Pt atom as its fifth ligand. The bilinear Eyring plot is interpreted as due to the existence of an additional mechanism for the exchange of the edges of the pyridine ligand, which dominates at high temperatures. It is characterized by a high enthalpy of activation and an exceedingly high entropy of activation. We propose that it involves a reversible substitution of the pyridine ligand on one or two adjacent square planar Pt cations by the counterion, which results in an opening of the cage and allows the pyridine to rotate freely until the bond recloses and the prism reforms. The proposed reaction is thus the reverse of the last expected step of the original self-assembly, about whose mechanism nothing is known, but which could proceed in a way similar to that proposed for the self-assembly of a much larger dodecahedron.[35]

Prompted by the results of molecular dynamics calculations, we performed a simple calculation of the entropy of cavitation in nitromethane. This accounts for the unusually highly favorable activation entropy quantitatively by suggesting that it is due to the expansion of the nitromethane solvent into a vapor bubble that is normally present at equilibrium inside the internally nonpolar prism **3c**. The agreement is undoubtedly partly accidental, and some of the positive value of $\Delta S^{\ddagger}$ is surely

(32) Chapman, K. T.; Still, W. C. *J. Am. Chem. Soc.* **1989**, *111*, 3075.
(33) Smeets, R. M. M.; Keyser, U.; Wu, M. Y.; Dekker, N. H.; Dekker, C. *Phys. Rev. Lett.* **2006**, *97*, 088101.
(34) Liu, P.; Huang, X.; Zhou, R.; Berne, B. J. *Nature* **2005**, *437*, 159.
(35) Levin, M. D.; Stang, P. J. *J. Am. Chem. Soc.* **2000**, *122*, 7428.
(36) King, B. T.; Körbe, S.; Schreiber, P. J.; Clayton, J.; Havlas, Z.; Vyakaranam, K.; Fete, M. G.; Zharov, I.; Ceremuga, J.; Michl, J. *J. Am. Chem. Soc.* **2007**, *129*, 12960.

attributable to a floppiness of the open structure. The presence of gaseous solvent bubbles inside molecular cages may be a general phenomenon and appears to be worth further investigation. One can envisage a relation to the inclusion of guest molecules, to the ease with which the cages assemble with and without templates and, in a more general sense, to protein unfolding.

Experimental Section

The salt Cs^+ 1-H-$CB_{11}Me_{11}^-$ was prepared according to known procedures.[36] All NMR experiments were performed and analyzed as described in the preceding companion paper.[1]

Calculations. All geometries were minimized with the TINK[6] program using the UFF force field.[4] Charges were calculated by charge equilibration.[5] VMD,[37] Moil-View,[38] Povray,[39] and Materials Studio[40] were used for molecular graphics. Calculation of the rotational barrier of pyridine around a Pt−N bond was accomplished by simulation of two complete rotations in 1° increments. Rotation in the opposite direction gave the same torsional barrier trajectory with respect to the dihedral angle between the platinum coordination plane and the pyridine ring. The TINK[6] program and charge equilibration were also used to perform constant energy molecular dynamics simulations (room temperature, 500 ps, 1 fs time step, 15–30 Å cutoff, ~20 simulations total). VMD[37] and a commercial video processing program VideoMach[41] were used to generate computer animations from molecular dynamics trajectories.

Acknowledgment. Dedicated to Prof. Rudolf Zahradník on the occasion of his 80th birthday. Financial support from the National Science Foundation (CHE-0306720, CHE-0446688, and OISE 0532040), the USARO (DAAD19-01-1-0521), DoD High Performance Modernization Office (Challenge Project C1R and ARONC014), the European Commission (STRP NMP4-013880 and MCRTN-CT-2005-019481), the GAAV (IAA400550616), and Ministry of Education of the Czech Republic (KONTAKT ME-857) is gratefully acknowledged.

Note Added in Proof. It has recently been proposed that bubble formation and disappearance may be critical for the function of biological ion channels and anesthetic action of inert gases: Roth, R.; Gillespie, D.; Nonner, W.; Eisenberg, B. *Biophys. J.* BioFAST, published on January 30, 2008 as doi: 10.1529/biophysj.107/120493.

JA801341M

(37) Humphrey, W.; Dalke, A.; Schulten, K. *J. Mol. Graphics* **1996**, *14*, 33.
(38) Simmerling, C.; Elber, R.; Zhang, J. In *Modelling of Biomolecular Structures and Mechanisms*, Proceedings of the 27th Jerusalem Symposium on Quantum Chemistry and Biochemistry, Jerusalem, Israel, May 23–26, 1994; Pullman, A., Jortner, J., Pullman B., Eds.; Kluwer Academic Publishers: Dordrecht, The Netherlands, 1995; p 241.
(39) Persistence of Vision Pty. Ltd. (2004). Persistence of Vision (TM) Raytracer. Persistence of Vision Pty. Ltd., Williamstown, Victoria, Australia (http://www.povray.org).
(40) *Materials Studio 4.1*; Accelrys Software Inc.: San Diego, CA, 2006.
(41) VideoMach: Computer program that uses high performance media processing engine with ability to construct, join, split, filter, tune, and convert digital video, audio, images and image sequences, gromada.com, 2007 (http://gromada.com/).